Journal of Applied Pharmaceutical Science Vol. 13(Suppl 1), pp 034-040, September, 2023
Available online at http://www.japsonline.com
DOI: 10.7324/JAPS.2023.134301
ISSN 2231-3354

Computational design for the development of natural molecules as compelling inhibitors against the target SARS-CoV-2: An *in-silico* attempt

Nagarjuna Palathoti[1], Kalirajan Rajagopal[1*], Gowramma Byran[1], Kannan Raman[1], Edwin Jose[2], Manikandan Gurunathan[3]

[1]Department of Pharmaceutical Chemistry, JSS College of Pharmacy, JSS Academy of Higher Education & Research, Ooty, India.
[2]Department of Pharmaceutical Chemistry, Sankaralingam Bhuvaneswari College of Pharmacy, Sivakasi, India.
[3]Department of Mechanical Engineering, Velammal College of Engineering and Technology, Madurai, India.

ARTICLE INFO

Received on: 27/02/2023
Accepted on: 18/07/2023
Available Online: 20/09/2023

Key words:
SARS CoV-2, RdRp, supernatural database, MM-GBSA, docking studies, MD simulation, COVID-19.

ABSTRACT

A threat to the global human population has been established by the COVID-19 pandemic in 2020 and it is quite challenging to identify innovative medications in this epidemic. These are zoonotic and can potentially create massive outbreaks of illnesses that can result in morbidity and death. As a consequence, natural therapies for the anticipation and dealing of COVID-19 are widely acknowledged as a quick means to find successful therapeutic choices that can be found through *in-silico* drug screening tests. RNA-dependent RNA polymerase (RdRp), a vital precursor involved in the virus's life cycle, is present in SARS-CoV-2. Blocking the formation of the RdRp–RNA complex inhibits viral replica and boosts the immune response of the host. In our present research, with the use of a SuperNatural Database, we started the high-throughput virtual screening method to recognize inhibitors aiming for SARS-CoV-2 RdRp. According to extra-precision docking data, two compounds, SN00293542 and SN00391842 had −14.79 and −14.65 kcal/mol docking scores, respectively. In addition, Prime molecular mechanics generalized bond surface area research has identified hydrophobic energy and Van der Waal energy footings as significant contributions towards total binding free energy. Additionally, a hundred nanosecond Molecular dynamics simulation of the SN00391842/7D4F complex was run to determine its dynamic behavior.

INTRODUCTION

The large genus of enclosed coronaviruses is a single-stranded positive-sense RNA virus (CoVs) (V'kovski *et al*., 2021) that can infect people and are zoonotic and have the probability to create massive outbursts of illnesses that can cause morbidity and mortality. The viral pneumonia outbreaks in Wuhan in 2019 and 2020 are instigated (Lakshmi and Suresh, 2020) by an anew discovered Coronavirus illness. It is mainly spread with droplets produced by infested individuals while coughing, sneezing, or exhaling. Simple colds to serious respiratory conditions including severe acute respiratory syndrome are among the symptoms of the recently identified coronavirus (Adithya *et al*., 2021) COVID-19. There are approximately 4 million fatalities and 175 million sick cases documented globally. With 44 million active belongings and 0.53 million fatalities (WHO, 2023), India is experiencing a daily increase in coronavirus infections. In the face of a viral pandemic that is scattering as wildfire and an inadequate treatment reserve, we needed to quickly find novel beneficial agents with clinical applications (Umakanthan *et al*., 2020). Natural products have been generally accepted as chemical entities for therapeutic application from their inception as a foundation and source of modern medications. Natural chemicals' pharmacological and therapeutic properties with low toxicity play a significant role in the creation of additional effective medications (Rajagopal *et al*., 2019). Herein current study, we want to high spot the unrealized potential of plant-based natural

**Corresponding Author*
Kalirajan Rajagopal, Department of Pharmaceutical Chemistry, JSS Academy of Higher Education & Research, JSS College of Pharmacy, Ooty, India.
E-mail: rkalirajan @ jssuni.edu.in

compounds as antiviral drug medications. The nucleocapsid (N), spike (S), membrane protein (M), and envelop proteins (E), as well as proteases, hemagglutinin esterases, helicases, and other proteins involved in the viral entrance, the existence, and reproduction, were used to build the viral structure (Kumar *et al.*, 2021; Mielech *et al.*, 2014). The nonexistence of proteins in human equivalents makes them interesting targets (Raj, 2021; Yadav *et al.*, 2021). The SARS-CoV-2 core Rd-RNA polymerase (RdRp) is made up of the non-structural protein nsp12, and two accessary subunits (nsp7 and nsp8). The SARS-CoV-2 virus contains RdRp, an essential enzyme involved in the viral life cycle (Lei *et al.*, 2018; Lim *et al.*, 2000; Osipiuk *et al.*, 2021). Blocking the formation of the RdRp complex inhibits viral replica and enhances the immune response of the host, so limiting its spread (Yin *et al.*, 2021). We have attempted to design and assessed several molecules for their biological activities such as anticancer, anti-SARS CoV-2, and others as a component of our ongoing research and utilized *in silico* and wet lab approaches for the discovery of dynamic molecules (Kalirajan *et al.*, 2017) for various biological activities (Kalirajan, 2020; Kalirajan *et al.*, 2012a, 2012b, 2018, 2019a, 2019b, 2020). The current work attempts to find inhibitors against RdRp utilizing the high-throughput virtual screening (HTVS) procedure by utilizing the SuperNatural Database, which contains 4,00,000 natural chemicals (Rajagopal *et al.*, 2021). The binding modes were identified using consecutive docking of HTVS, standard precision (SP), and Extra-Precision (XP) modes. To recognize natural drug-bound patterns in the RdRp active site, further molecular mechanics generalized bond surface area (MM-GBSA) and Molecular dynamics (MD) simulations (Ram *et al.*, 2022).

MATERIALS AND METHODS

HTVS and molecular docking

Molecular docking is a bioinformatic modeling approach used to predict the three-dimensional conformer

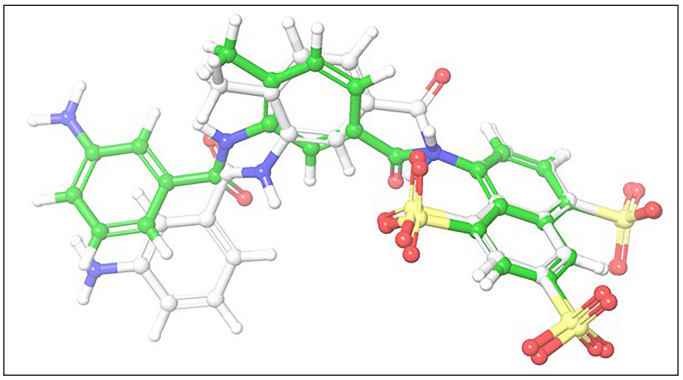

Figure 1. Superimposition of native and docked conformer H3U.

Table 1. Molecular docking score (XP) in the active site of RdRp (kcal/mol) (7D4F.pdb).

S.no	Compound code	Glide score	Glide model	Glide evdw	Glide_ecoul	Glide_energy
1	SN00293542	−14.79	−90.10	−31.41	−32.18	−63.60
2	SN00391842	−14.65	−115.2	−54.53	−30.58	−85.12
3	SN00216715	−14.64	−39.02	−26.19	−40.76	−66.96
4	SN00340755	−14.44	−123.8	−60.29	−23.14	−83.43
5	SN00334894	−14.06	−79.32	−32.64	−32.13	−64.77
6	105404-83-9	−13.63	−100.2	−47.51	−33.75	−81.26
7	SN00299979	−12.31	−134.6	−59.80	−35.76	−95.56
8	SN00338961	−12.23	−103.2	−55.35	−25.91	−81.26
9	865369-05-7	−12.20	−76.74	−49.23	−21.20	−70.43
10	SN00352807	−11.78	−48.35	−34.96	−25.04	−60.01
11	SN00382588	−10.82	−88.24	−35.15	−29.62	−64.77
12	SN00213037	−10.72	−76.36	−29.30	−34.67	−63.97
13	SN00216711	−10.54	−56.85	−27.34	−22.43	−49.77
14	SN00040401	−10.13	−76.52	−31.27	−24.51	−55.78
15	96626378	−10.04	−101.0	−47.56	−22.10	−69.66
16	SN00213304	−9.88	−71.49	−38.19	−28.68	−66.88
17	SN00296151	−9.58	−61.31	−19.86	−28.09	−47.95
18	SN00350811	−9.57	−81.82	−31.55	−27.40	−58.96
19	SN00392377	−9.36	−62.33	−27.46	−23.94	−51.40
20	SN00216726	−9.15	67.10	−28.30	−7.86	−36.17
21	5280805	−9.13	−65.73	−36.08	−19.39	−55.48
22	Co-crystal	−5.37	−86.62	−39.57	−18.54	−58.12
23	Remdesivir	−5.05	−63.36	−39.77	−14.83	−54.61

of any complex and generates different possible conformers that are ranked and grouped using a scoring function in the software. Docking simulations predict optimized docked conformers based on the system's total energy (Dar and Mir, 2017). Using the protein preparation wizard of Schrödinger Suite LLC, (Sastry *et al*., 2013) the three-dimensional X-ray crystal structure of RdRp with co-crystal suramin (7D4F.pdb) (Yin *et al*., 2021), which was retrieved from the research collaboratory for structural bioinformatics, was further created. Removed crystalized water and modified bond ordering with hydrogen additions, the protein was produced (Sukumaran *et al*., 2020). Using Prime at pH 7.0, missing side chains and loops were added to produce protonation and tautomeric states for acidic and basic residues. Protein was optimized using the molecular force field OPLS4 (potential optimized for liquid simulations) and the crystallographic heavy atom root mean square deviation (RMSD) was set to 0.30 Å. A grid box ($x = 52.5$; $y = 31.1$; $z = -0.61$) was constructed at the active site around the cocrystal using a van der Waals scaling of 0.80 for the receptor, and 0.16 was used as the partial charge limit. We obtained three-dimensional conformers of 4,00,000 natural chemicals (Dunkel *et al*., 2006) using the SuperNatural database. The computer-generated roadmap started by preparing ligands using Ligprep and using the prefilter option to remove excess. Using default settings for HTVS, SP, and XP modes, ligands were sequentially docked into RdRp catalytic pocket (7D4F.pdb). The ideal docked position was selected using hydrogen bond, glide score, and glide energy evaluations.

Total free energy calculation using prime MM-GBSA

The generalized-born surface area (GBSA) continuum solvent model and prime MM-GBSA methods were used to calculate the ligand-protein complex binding contributions of enthalpy and entropy-associated mechanisms (Naresh *et al*., 2020). The equation was used to estimate (in kcal/mol) molecular mechanics energy, and polar and nonpolar solvation contributions from components (Shivakumar *et al*., 2010).

$\Delta G_{bind} = G_{complex} - G_{protein} - G_{ligand}$

ΔG_{bind} = binding free energy of complex Calculated.

$G_{complex}$ = Binding free energy of complex minimized.

$G_{protein}$ = Binding free energy of receptor.

G_{ligand} = Binding free energy of ligand unbound.

Table 2. MM-GBSA binding free energy values (kcal/mol) for the obtained hits in the active site of RdRp (kcal/mol) (7D4F.pdb).

S.no	Compound code	ΔG Bind	ΔG Coulomb	ΔG Hbond	ΔG Lipo	ΔG vdW
1	SN00299979	−164.84	−131.78	−17.35	−27.43	−64.25
2	SN00391842	−155.86	−178.30	−18.25	−24.55	−66.80
3	SN00338961	−143.06	−154.37	−15.38	−19.41	−67.19
4	SN00340755	−142.92	−87.86	−16.20	−20.20	−59.17
5	105404-83-9	−138.75	−191.13	−17.09	−20.89	−57.93
6	865369-05-7	−121.53	−134.53	−15.11	−21.67	−53.57
7	SN00213037	−110.68	−139.35	−17.85	−10.19	−38.47
8	SN00216711	−108.80	−76.08	−14.32	−5.01	−10.47
9	96626-37-8	−105.31	−97.93	−18.84	−19.20	−44.87
10	SN00382588	−100.51	−108.64	−16.72	−19.72	−24.97
11	SN00352807	−91.44	−93.12	−11.80	−12.07	−40.18
12	SN00040401	−88.08	−100.36	−10.85	−21.69	−30.79
13	SN00216715	−70.81	−35.34	−9.57	−4.61	−29.75
14	SN00334894	−56.99	−80.31	−9.55	−4.05	−4.25
15	SN00293542	−41.31	−38.0	−10.18	−6.46	−36.01

Table 3. The number of hydrogen bonds and intermingling amino acid residues for the top 5 hits in the catalytic pocket of RdRp enzyme (7D4F.pdb).

S.no	Compound code	Number of hydrogen bonds	Interacting amino acid residues
1	SN00299979	10	Asn496, Asn497, Arg569, Lys577, Thr593, Asp684, Arg836, Asp865
2	SN00391842	6	Asn497, Lys577, Gly590, Thr591, Tyr689
3	SN00338961	5	Asn497, Lys500, Gly590, Lys593, Ser682
4	SN00340755	8	Lys500, Gly590, Ser592, Ser682, Asp684, Ala688, Ser759, Arg836
5	105404-83-9	10	Asn496, Lys500, Arg569, Lys577, Arg583, Gly590, Lys593, Tyr689

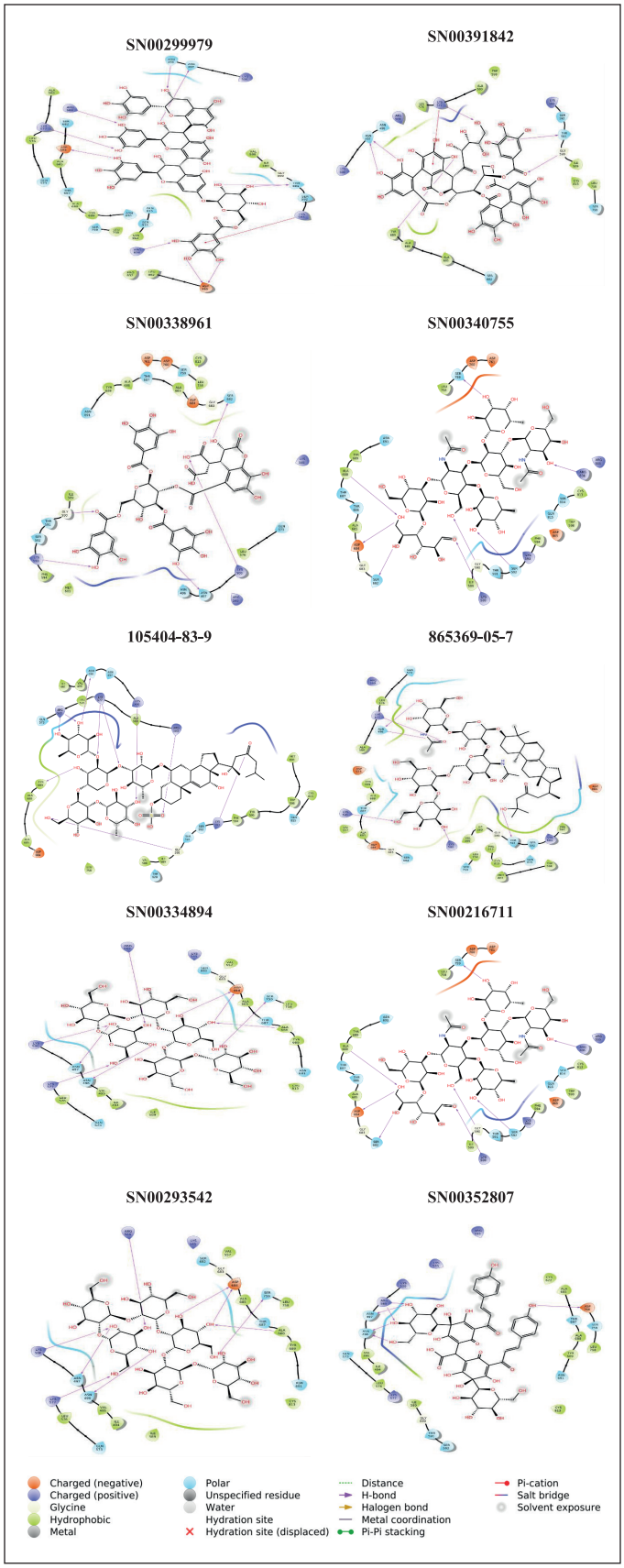

Figure 2. 2D-interaction diagrams of top 10 compounds in the catalytic pocket of RdRp enzyme (7D4F.pdb).

MD simulation study

We employed the Schrödinger, LLC, New York, Desmond module to perform MD simulation to analyze the binding behavior of top-ranked molecules at the nuclear level and to comprehend the molecular interface investigation (Bowers *et al*., 2006; Jorgensen *et al*., 1983). The complex SN00391842/7D4F was solvated using the TIP4P water model (Essmann *et al*., 1995) with orthorhombic periodic boundaries and a 10 Å of buffer zone between protein atoms and box edges. The generated system was neutralized with the addition of 0.15 Molar NaCl counter ions. The OPLS4 force field settings were then used to minimize the system (Harder *et al*., 2016). With a 1e-09 tolerance, long-range electrostatic interactions were calculated using the Smooth Particle Mesh Ewald method. At a cut-off radius of 9.0 Å, the short-range Vander Waals and Coulomb interactions were estimated. In an isothermal-isobaric ensemble, 100 ns of MD simulations at 2 fs a time step were run at 300 Kelvin and 1 bar of pressure [Simulation of system based on constant number (N), and constant-temperature (T), but pressure (P) is regulated]. The Martyna–Tobias-Klein barostat and Nose–Hoover thermostat chain thermostat techniques are merged at 100 and 200 ps (Martyna *et al*., 1992, 1994). Reference system propagator algorithm multiple time-step algorithms were employed for bonded, non-bonded short-range, and long-range electrostatic forces, respectively. Data was gathered, and the resulting trajectories were analyzed for every 100 ps (Kalirajan, 2020; Kalirajan *et al*., 2017, 2020).

RESULTS AND DISCUSSION

Molecular docking and total binding free energy calculation

Using a structural-based virtual screening technique from the Schrödinger suite, the RdRp (7D4F.pdb) enzyme was utilised to screen a library of 400,000 molecules from the SuperNatural Database. Initial prefilters were used in the virtual screening method to exclude ligands containing reactive functional groups according to Lipinski's rule. Three accuracy stages of the sequential docking methodology (HTVS, SP, and XP docking) were carried out while maintaining default constraints. A final 21 compounds were identified after visually analyzing the bound postures and hydrogen bond establishment for the high-ranked hits during XP mode. With the help of the virtual screening protocol, several different scaffold topologies were discovered, such as 2-phenyl chromene rings allied with sugar moieties, pyrazinyl hexanoic acid, cyclohexyl dihydrogen phosphates allied with sugars, tetrahydroxy hexanal allied with pyran, benzyloxy benzoates allied with pyranoacetates and dicarbamimidamido pyran trihydroxy benzoates, etc. In the present research work, the docking protocol was validated by performing the re-dock with the co-crystal structure in the catalytic pocket of 7D4F and from the re-docked results, the RMSD for the superimposition of native and docked conformer revealed as 3.7 Å (Fig. 1). Thus, the docking protocol was considered good enough for replicating the docking results similar to the co-crystal structure and can consequently be applied for further molecular docking analysis. Tables 1 and 2 provided the glide scores and MM-GBSA energy scores. Selected first top 5 XP docked pose hits showed 5–10 hydrogen bonding, the most observed bonds by all the phytoconstituents (Table 3). Table 1 shows that the glide score ranges from −14.79

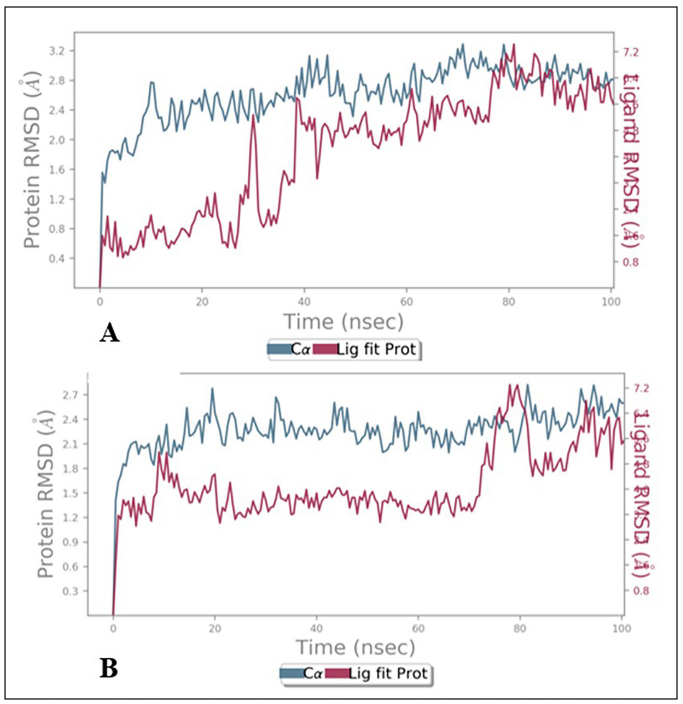

Figure 3. RMSD graph for (A) H3U/7D4F complex (B) SN00391842/7D4F complex.

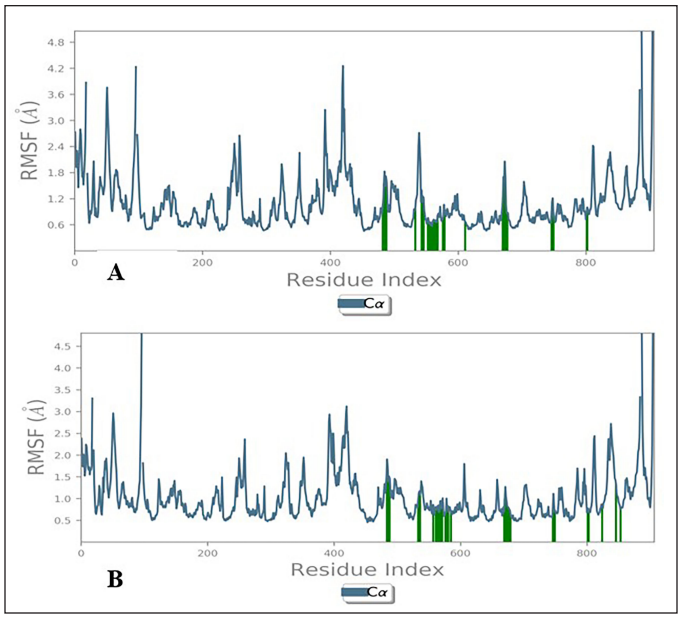

Figure 4. RMSF graph for (A) H3U/7D4F complex (B) SN00391842/7D4F complex.

to −9.13 kcal/mol. The post-docking minimized binding free energies (ΔBind) of the highest scoring poses of the selected hits ranged from −41.31 to −155.86 Kcal/mol. The significant Van der Waal energy terms (ΔVdW) −36.01to −64.25 Kcal/mol and the moderately favored hydrophobic energy terms (ΔLipo) −6.46 to −27.43 Kcal/mol favor total binding energy, as seen in Table 2. The hits SN00293542 and SN00391842 had the highest

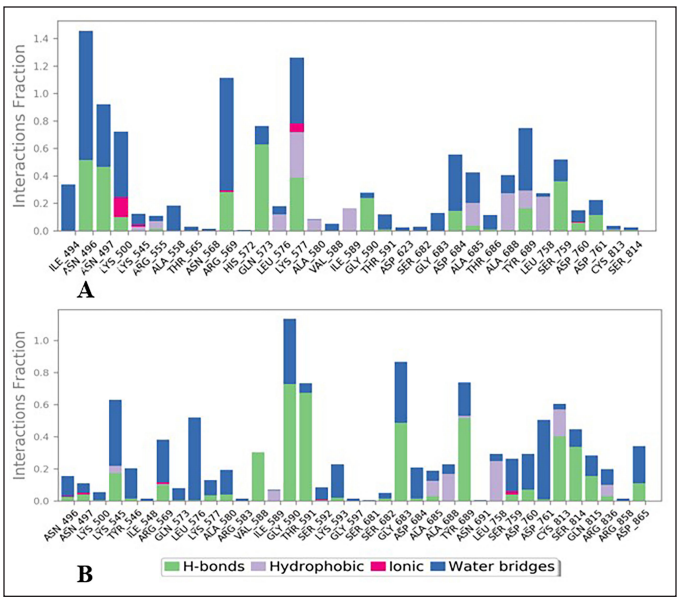

Figure 5. Protein-ligand contacts profile for (A) H3U/7D4F complex (B) SN00391842/7D4F complex.

glide scores of −14.79 and −14.65 kcal/mol. Conferring to the binding free energy calculation MMGB-SA approach, compounds SN00299979 and SN00391842 had the highest binding affinity with −164.84 and −155.86 kcal/mol respectively. Figure 2 shows the 2D interactions of the top 10 hits. Compound SN00391842 had taken for further study by considering the both docking score and binding affinity.

MD simulation

Both H3U(cocrystal)/7D4F and the docked pose SN00391842/7D4F complexes underwent 100 nanoseconds of MD simulation. During simulation, from Figure 3A and B, it was observed that the protein Cα atoms were for both H3U/7D4F and the docked pose SN00391842/7D4F stabilized throughout the simulation with a minimum RMSD of 2.3 to 3.2 Å 2.1 to 2.7 Å respectively and in Figure 3A for the ligand during the initial 42 ns, minimal fluctuations were observed and after that stabilized up to 80 ns and again fluctuations were observed with RMSD 5.6 to 7.2 Å whereas in Figure 3B for the ligand during the initial 15 ns, minimal fluctuations were observed and after that stabilized up to 75 ns and again fluctuations were observed with RMSD 4.7 to 7.2 Å. From Figure 4A and B, we can observe that fluctuations with root mean square fluctuations (RMSF) of 0.6 to 4.2 Å and 0.5 to 4.7 Å respectively maintained throughout the simulation but whenever the ligand atoms bound to the particular amino acids there, we can notice the minimum fluctuations i.e. from 500 to 580, 700 to 750, 800 to 900 amino acids with 0.8 to 1.4, 0.6 to 1.3 and 0.7 to 1.3 Å respectively. In Figures 5A and B, most amino acids in the catalytic pocket have maintained their interaction as hydrogen bonds and water bridges, and most of them have demonstrated multiple interactions. Figure 6A and B, Asn496, Asn497, Arg569, Gln573, Lys577, Tyr689, Gly 590, Thr591, Gly683, Tyr689, and Cys813 are these particular

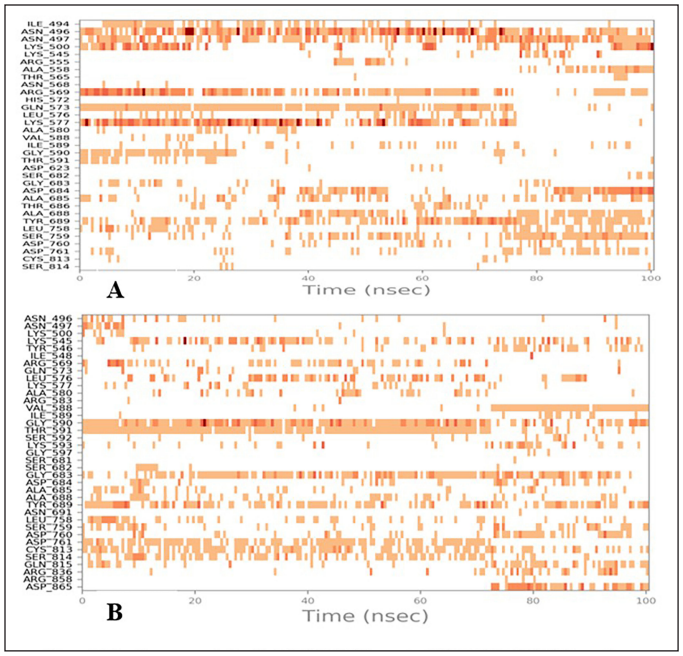

Figure 6. Timeline representation for (A) H3U/7D4F complex (B) SN00391842/7D4F complex.

amino acids that maintained continuous and multiple contacts with the ligand atoms throughout the simulation. From the deposited data, we can notice that the SN00391842/7D4F complex attained more stability while performing the triplicate with a different random seed number. With this, we may suggest that these natural chemical entities would act as scaffolds for the development of new drugs in the future for the management of COVID-19.

CONCLUSION

There have been approximately reported 174 million cases of infection and 3.75 million fatalities worldwide. There are currently 4 million coronavirus cases active in India, and there have been 0.5 million fatalities. The current investigation aims to find inhibitors that target the RdRp enzyme, which is essential for viral replication and growth. Using the SuperNatural database of 400,000 natural chemicals as part of an HTVS process, we used HTVS, SP, and XP docking modes. Then sequential docking technology was introduced. The top 28 hit compounds were found after docking optimization. According to the XP docking results 2 molecules, SN00293542 and SN00391842 had glide scores of −14.79 and −14.65 kcal/mol, respectively. According to the MM-GBSA investigations, VanderWaal energy (ΔVdW) ranges from −36.01 to −64.25 kcal/mol while the hydrophobic energy terms (ΔLipo) range from −6.46 to −27.43 kcal/mol. According to 100 ns MD simulations, the SN00391842/7D4F complex was maintained in the catalytic pocket by hydrogen-bonding, hydrophobic, and water-bonding interactions. MD simulations for the trajectory SN00391842/7D4F were validated by performing the dynamic simulations in triplicate with random seed and the data was deposited. To further the development of possible SARS-CoV-2 inhibitors, *in silico* studies that are now underway might be beneficial.

ACKNOWLEDGMENT

The authors also thank "All India Council for Technical Education, Government of India for sanctioned- project under Drug Discovery hackathon-2020 for covid drug discovery Phase-II research (F.No. 1-1 / IC /DDH / 2020-21)."

AUTHOR CONTRIBUTIONS

All authors made substantial contributions to conception and design, acquisition of data, or analysis and interpretation of data; took part in drafting the article or revising it critically for important intellectual content; agreed to submit to the current journal; gave final approval of the version to be published; and agree to be accountable for all aspects of the work. All the authors are eligible to be an author as per the international committee of medical journal editors (ICMJE) requirements/guidelines.

CONFLICTS OF INTEREST

The authors report no financial or any other conflicts of interest in this work.

ETHICAL APPROVALS

This study does not involve experiments on animals or human subjects.

DATA AVAILABILITY

All data generated and analyzed are included in this research article.

PUBLISHER'S NOTE

This journal remains neutral with regard to jurisdictional claims in published institutional affiliation.

REFERENCES

Adithya J, Nair B, Aishwarya TS, Nath LR. The plausible role of Indian traditional medicine in combating coronavirus (SARS-CoV 2): a mini-review. Curr Pharm Biotechnol, 2021; 22(7):906–19.

Bowers KJ, Chow E, Xu H, Dror RO, Eastwood MP, Gregersen BA, Klepeis JL, Kolossvary I, Moraes MA, Sacerdoti FD, Salmon JK. Scalable algorithms for molecular dynamics simulations on commodity clusters. In: Proceedings of the 2006 ACM/IEEE Conference on Supercomputing, LLC, New York, 2006, pp 84–es.

Dar AM, Mir S. Molecular docking: approaches, types, applications and basic challenges. J Anal Bioanal Tech, 2017; 8(2):1–3.

Dunkel M, Fullbeck M, Neumann S, Preissner R. Supernatural: a searchable database of available natural compounds. Nucleic Acids Res, 2006; 34(suppl_1):D678–83.

Essmann U, Perera L, Berkowitz ML, Darden T, Lee H, Pedersen LG. A smooth particle mesh Ewald method. J Chem Phys, 1995; 103:8577–93.

Harder E, Damm W, Maple J, Wu C, Reboul M, Xiang JY, Wang L, Lupyan D, Dahlgren MK, Knight JL, Kaus JW, Cerutti DS, Krilov G, Jorgensen WL, Abel R, Friesner RA. OPLS3: a force field providing broad coverage of drug-like small molecules and proteins. J Chem Theory Comput, 2016; 12:281–96.

Jorgensen WL, Chandrasekhar J, Madura JD, Impey RW, Klein ML. Comparison of simple potential functions for simulating liquid water. J Chem Phy, 1983; 79:926–35.

Kalirajan R. Activity of some novel chalcone substituted 9-anilinoacridines against coronavirus (COVID-19): a computational approach. Coronaviruses, 2020; 1(1):13–22.

Kalirajan R, Gaurav K, Pandiselvi A, Gowramma B, Sankar S. Novel thiazine substituted 9-anilinoacridines: synthesis, antitumour activity and structure activity relationships. Anticancer Agents Med Chem, 2019b; 19:1350–8.

Kalirajan R, Gowramma B, Srikanth J, Vadivelan R. Activity of phytochemical constituents of black pepper, ginger and garlic against coronavirus (COVID-19): an *in-silico* approach. Int J Health Allied Sci, 2020; 9:S43–50.

Kalirajan R, Muralidharan V, Jubie S, Gowramma B, Gomathy S, Sankar S, Elango K. Synthesis of some novel pyrazole substituted 9-anilinoacridine derivatives and evaluation for their antioxidant and cytotoxic activities. J Heterocycl Chem, 2012a; 49:748–54.

Kalirajan R, Pandiselvi A, Gowramma B, Balachandran P. *In-silico* design, ADMET screening, MM-GBSA binding free energy of some novel isoxazole substituted 9-anilinoacridines as HER2 inhibitors targeting breast cancer. Curr Drug Res Rev, 2019a; 11:118–28.

Kalirajan R, Sankar S, Jubie S, Gowramma B. Molecular docking studies and *in-silico* ADMET screening of some novel oxazine substituted 9-anilinoacridines as topoisomerase II inhibitors. Indian J Pharm Educ Res, 2017; 51:110–5.

Kalirajan R, Vivekkulshrestha V, Sankar S, Jubie S. Docking studies, synthesis, characterization of some novel oxazine substituted 9-anilinoacridine derivatives and evaluation for their anti-oxidant and anticancer activities as topoisomerase II inhibitors. Eur J Med Chem, 2012b; 56:217–24.

Kalirajan R, Vivekkulshrestha V, Sankar S. Synthesis, characterization and evaluation for antitumour activity of some novel oxazine substituted 9-anilinoacridines and their 3D-QSAR studies. Indian J Pharm Sci, 2018; 80:921–9.

Kumar R, Harilal S, Al-Sehemi AG, Pannipara M, Behl T, Mathew GE, Mathew B. COVID-19 and domestic animals: exploring the species barrier crossing, zoonotic and reverse zoonotic transmission of SARS-CoV-2. Curr Pharm Des, 2021; 27:1194–201.

Lakshmi SP, Suresh M. Factors influencing the epidemiological characteristics of pandemic COVID-19: a TISM approach. Int J Healthc Manag, 2020; 13:89–98.

Lei J, Kusov Y, Hilgenfeld R. Nsp3 of coronaviruses: structures and functions of a large multi-domain protein. Antiviral Res, 2018; 149:58–74.

Lim KP, Ng LF, Liu DX. Identification of a novel cleavage activity of the first papain-like proteinase domain encoded by open reading frame 1a of the coronavirus avian infectious bronchitis virus and characterization of the cleavage products. J Virol, 2000; 74:1674–85.

Martyna GJ, Klein ML, Tuckerman M. Nose-Hoover chains: the canonical ensemble via continuous dynamics. J Chem Phys, 1992; 97:2635–43.

Martyna GJ, Tobias DJ, Klein ML. Constant pressure molecular dynamics algorithms. J Chem Phys, 1994; 101:4177–89.

Mielech AM, Chen Y, Mesecar AD, Baker SC. Nidovirus papain-like proteases: multifunctional enzymes with protease, deubiquitinating and deISGylating activities. Virus Res, 2014; 194:184–90.

Naresh P, Selvaraj A, Shyam Sundar P, Murugesan S, Sathianarayananan S, Namboori PKK, Jubie S. Targeting a conserved pocket (n-octylb-Dglucoside) on the dengue virus envelope protein by small bioactive molecule inhibitors. J Biomol Struct Dyn, 2020; 0:1–13.

Osipiuk J, Azizi SA, Dvorkin S, Endres M, Jedrzejczak R, Jones KA, Kang S, Kathayat RS, Kim Y, Lisnyak VG, Maki SL, Nicolaescu V, Taylor CA, Tesar C, Zhang YA, Zhou Z, Randall G, Michalska K, Snyder SA, Dickinson BC, Joachimiak A. Structure of papain-like protease from SARS-CoV-2 and its complexes with non-covalent inhibitors. Nat Commun, 2021; 12:743.

Raj R. Analysis of non-structural proteins, NSPs of SARS-CoV-2 as targets for computational drug designing. Biochem Biophys Rep, 2021; 25:100847.

Rajagopal K, Varakumar P, Aparna B, Byran G, Jupudi S. Identification of some novel oxazine substituted 9-anilinoacridines as SARS-CoV-2 inhibitors for COVID-19 by molecular docking, free energy calculation and molecular dynamics studies. J Biomol Struct Dyn, 2021; 39(15):5551–62.

Rajagopal K, Varakumar P, Baliwada A, Byran G. The activity of phytochemical constituents of *Curcuma longa* (turmeric) and *Andrographis paniculata* against coronavirus (COVID-19): an *in-silico* approach. Futur J Pharm Sci, 2019; 6:104.

Ram TS, Munikumar M, Raju VN, Devaraj P, Boiroju NK, Hemalatha R, Prasad PV, Gundeti M, Sisodia BS, Pawar S, Prasad GP. *In silico* evaluation of the compounds of the ayurvedic drug, AYUSH-64, for the action against the SARS-CoV-2 main protease. J Ayu Integr Med, 2022; 13(1):100413.

Sastry GM, Adzhigirey M, Day T, Annabhimoju R, Sherman W. Protein and ligand preparation: parameters, protocols, and influence on virtual screening enrichments. J Comput Aided Mol Des, 2013; 27:221–34.

Shivakumar D, Williams J, Wu Y, Damm W, Shelley J, Sherman W. Prediction of absolute solvation free energies using molecular dynamics free energy perturbation and the OPLS force field. J Chem Theory Comput, 2010; 6(5):1509–19.

Sukumaran S, Meghna M, Sneha S, Arjun B, Sathianarayanan S, Saranya TS. *Insilico* analysis of acridone against TNF-a and PDE4 targets for the treatment of psoriasis. Int J Res Pharm Sci, 2020; 11:1251–9.

Umakanthan S, Sahu P, Ranade AV, Bukelo MM, Rao JS, Abrahao-Machado LF, Dahal S, Kumar H, Kv D. Origin, transmission, diagnosis and management of coronavirus disease 2019 (COVID-19). Postgrad Med J, 2020; 96:753–58.

V'kovski P, Kratzel A, Steiner S, Stalder H, Thiel V. Coronavirus biology and replication: implications for SARS-CoV-2. Nat Rev Microbiol, 2021; 19:155–70.

WHO. 2023. Available via https:// covid19.who.int/region/searo/country/in (Accessed 03 January 2023).

Yadav R, Chaudhary JK, Jain N, Chaudhary PK, Khanra S, Dhamija P, Sharma A, Kumar A, Handu S. Role of structural and non-structural proteins and therapeutic targets of SARS-CoV-2 for COVID-19. Cells, 2021; 10:1–16.

Yin W, Luan X, Li Z, Zhou Z, Wang Q, Gao M, Wang X, Zhou F, Shi J, You E, Liu M. Structural basis for inhibition of the SARS-CoV-2 RNA polymerase by suramin. Nat Struct Mol Biol, 2021; 28(3):319–25.

How to cite this article:
Palathoti N, Rajagopal K, Byran G, Raman K, Jose E, Gurunathan M. Computational design for the development of natural molecules as compelling inhibitors against the target SARS-CoV-2: An *in-silico* attempt. J Appl Pharm Sci, 2023; 13(Suppl 1):034–040.